doi:10.1016/j.jmb.2008.08.078 J. Mol. Biol. (2008) 384, 109–119

JMB

Available online at www.sciencedirect.com

ScienceDirect

ELSEVIER

Computational Redesign of a Protein–Protein Interface for High Affinity and Binding Specificity Using Modular Architecture and Naturally Occurring Template Fragments

V. Potapov[1,2]†, D. Reichmann[2]†, R. Abramovich[2], D. Filchtinski[2], N. Zohar[2], D. Ben Halevy[2], M. Edelman[1]*, V. Sobolev[1]* and G. Schreiber[2]*

[1]*Department of Plant Science, Weizmann Institute of Science, Rehovot 76100, Israel*

[2]*Department of Biological Chemistry, Weizmann Institute of Science, Rehovot 76100, Israel*

Received 5 June 2008; received in revised form 24 July 2008; accepted 21 August 2008
Available online 9 September 2008

A new method is presented for the redesign of protein–protein interfaces, resulting in specificity of the designed pair while maintaining high affinity. The design is based on modular interface architecture and was carried out on the interaction between TEM1 β-lactamase and its inhibitor protein, β-lactamase inhibitor protein. The interface between these two proteins is composed of several mostly independent modules. We previously showed that it is possible to delete a complete module without affecting the overall structure of the interface. Here, we replace a complete module with structure fragments taken from nonrelated proteins. Nature-optimized fragments were chosen from 10^7 starting templates found in the Protein Data Bank. A procedure was then developed to identify sets of interacting template residues with a backbone arrangement mimicking the original module. This generated a final list of 361 putative replacement modules that were ranked using a novel scoring function based on grouped atom–atom contact surface areas. The top-ranked designed complex exhibited an affinity of at least the wild-type level and a mode of binding that was remarkably specific despite the absence of negative design in the procedure. In retrospect, the combined application of three factors led to the success of the design approach: utilizing the modular construction of the interface, capitalizing on native rather than artificial templates, and ranking with an accurate atom–atom contact surface scoring function.

Keywords: computational protein design; protein–protein interaction; structure-based reengineering; molecular recognition

Edited by M. Levitt

Introduction

The ability of proteins to specifically interact with one another is central to life. These interactions form networks, whose operations drive processes such as signal transduction, the immune system, control of enzyme reactions, cell differentiation, growth, and so on.[1] A major goal in studying protein–protein interfaces is to achieve a biophysical understanding from which engineering principles can be derived. Interface engineering opens up a myriad of possibilities for promoting or inhibiting cellular processes, both for biotechnological and biomedical purposes. At present, protein engineers can choose either to use rational computer-based design or *in vitro* protein evolution methods such as phage display and ribosomal display[2,3] to select effective binders. The procedures based on directed evolution and selection are technically demanding, but proved to be very successful in engineering binding proteins.[4]

*Corresponding authors. E-mail addresses: marvin.edelman@weizmann.ac.il; vladimir.sobolev@weizmann.ac.il; gideon.schreiber@weizmann.ac.il.

† V.P. and D.R. contributed equally to this work.

Abbreviations used: PDB, Protein Data Bank; TEM1, TEM1 β-lactamase; BLIP, β-lactamase inhibitor protein; M2, module 2; SPR, surface plasmon resonance.

Yet, they do not add to our understanding of the protein–protein binding mechanism. The ability to successfully design new interactions *in silico* requires at least a partial understanding of the binding process. It allows testing of design principles and, in the future, has a potential to become a viable way for engineering protein–protein interactions.[5] Therefore, the development of successful computational design methods, while challenging, is worthwhile.

Binding sites have previously been rationally redesigned; however, there exists no example for the design-from-scratch of a new binding site for transient heterocomplexes obtaining reasonably high affinity. In a number of cases, tighter binding to the wild-type partner[6–8] or new specificities for binding[9] were successfully achieved. Resolving the structures of designed interfaces teaches us that some design features were implemented as predicted, but others were not.[10] Thus, one problem in the design of new interfaces may be the inability to consistently produce accurate structural models, particularly if backbone movements are involved. A second challenge is the approximated nature of the energy functions used and the computational difficulty in achieving the absolute energy minimum due to the very large search space.

We previously showed that the interface between proteins is built in a modular fashion.[11,12] Each module is comprised of a number of closely interacting residues, with few interactions between modules. Single mutations cause complex energetic and structural consequences within their module. Yet, mutations in one module do not affect residues located in a neighboring one. As a result, the structural and energetic consequences of the deletion of

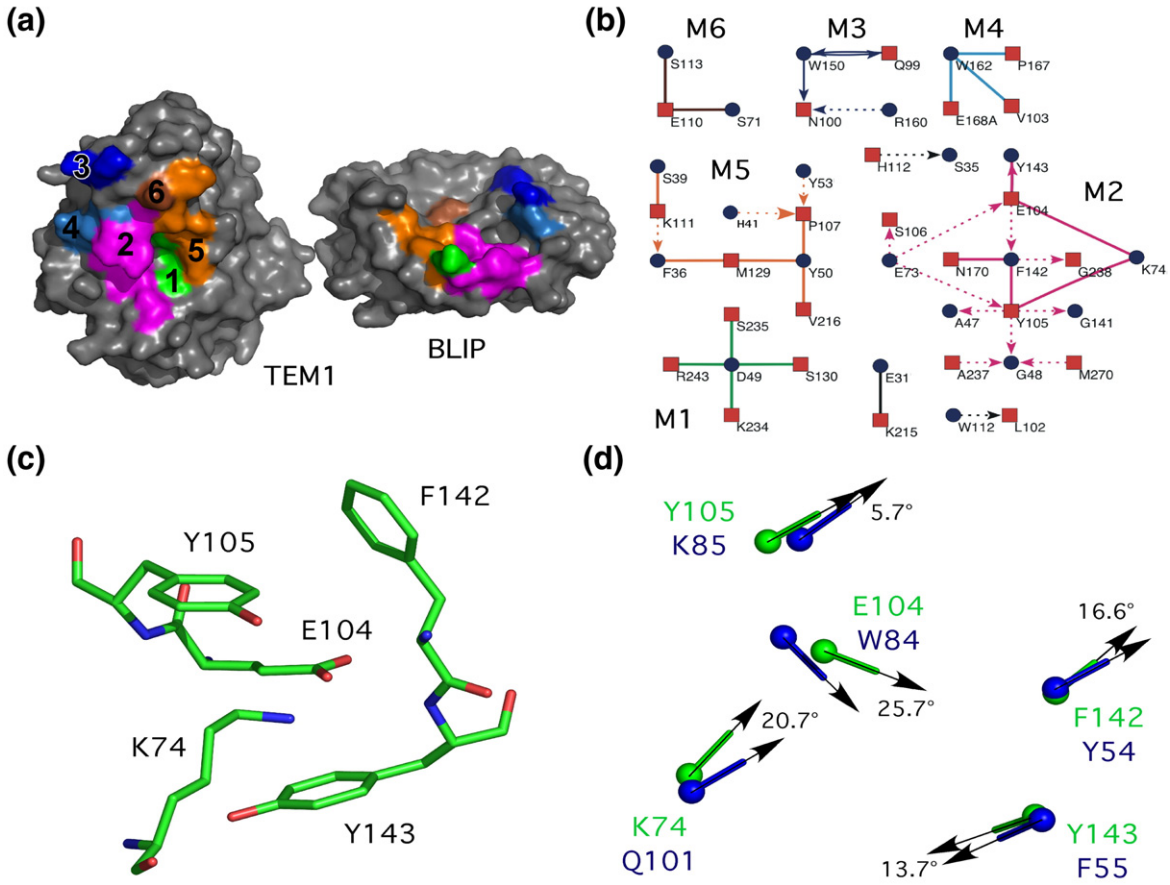

Fig. 1. Modular architecture of the TEM1–BLIP interface. (a) Location of modules on the protein surface of TEM1 and BLIP proteins (PDB ID 1JTG). The color scheme corresponds to that in (b). Numbers in TEM1 are for M1–M6. (b) Connectivity map of the wild-type TEM1–BLIP interface. TEM1 (squares) and BLIP (circles) residues are nodes. Three interaction types are shown: side chain/side chain (continuous lines), backbone/side chain (dotted lines), and cases where both side chain/side chain and backbone/side chain are found between the same pair of residues (continuous lines with arrows). The arrows point towards the residue that contributes the backbone to the interaction. The connectivity map was created as described in Reichmann *et al.*[11] and is color-coded to match the representation in (a). (c) Detailed structure of wild-type M2 (PDB ID 1JTG), the module chosen for interface design. (d) Superimposition of the highest-scoring PDB module (PDB ID 1IOO; in blue) and wild-type M2 (in green). All 45 distances between five C^{α} atoms and five C^{β} atoms in the PDB module are within 2.5 Å of the corresponding distances in M2. All five angles between C^{α} and C^{β} vectors are less than 30°. C^{α} atoms are represented as balls; sticks represent the covalent bonds between C^{α} and C^{β}. Labels in green indicate residues in wild-type M2, and labels in blue indicate the corresponding residues in the highest-scoring PDB module. Molecular graphics images were generated with PyMOL.[37]

entire modules are surprisingly small.[12] In this study, we present a new strategy to redesign protein–protein interfaces by taking advantage of their modular architecture. We suggest that such modules can be replaced with "ready-made" templates extracted from resolved Protein Data Bank (PDB) structures. We tested this idea for the interface of TEM1 β-lactamase (TEM1) with β-lactamase inhibitor protein (BLIP) and achieved high affinity and specificity for a designed mutant complex.

Results

The interface between the TEM1 and BLIP proteins is made up of six energetically independent modules.[11,12] In this study, we search for methods to redesign module 2 (M2), which is composed of residues Glu104 and Tyr105 in TEM1, and Lys74, Phe142, and Tyr143 in BLIP (Fig. 1). The crystal structure of the TEM1–BLIP complex in which the five residues composing M2 are mutated to Ala was solved[12] (PDB ID 1XXM), showing rigidity of the M2 environment (all-atom RMSD for interface residues equals 0.37 Å relative to wild type). Noteworthily, the large cavity created within the interface by mutational deletion of M2 was not filled with structural water.[12] The aim of our computational design is to fill this cavity with five new side chains, while providing high affinity and specificity for the designed complex. Two strategies are tested. One uses the RosettaDesign program to search for optimal residues.[13] RosettaDesign is among the most successful computational methods currently available.[8,9,14,15] The second utilizes resolved protein structures in the PDB as a source of "ready-made" nature-optimized residue fragments.

Redesign of the interface module using the RosettaDesign program

The RosettaDesign program was run 100 times, with each run providing a single solution comprising a double-TEM1 mutant and a triple-BLIP mutant (see Materials and Methods). All runs converged to eight different solutions, with each predicted to be energetically lower than the wild-type complex. Since energy scoring was not consistent for multiple solutions of the same residue set, we defined the best sets among the eight by their convergence (Fig. 2). The three sets with the highest degree of convergence were YN^{T}–NYP^{B}, EN^{T}–HYS^{B}, and EG^{T}–HYS^{B} (where superscript T marks mutations on TEM1 and superscript B marks mutations on BLIP). These were expressed, purified, and analyzed experimentally for binding using surface plasmon resonance (SPR) technology. The binding energies of the designed proteins are summarized in Table 1. Mutating simultaneously the five residues comprising M2 to alanine decreased the binding affinity by 14 kJ/mol and served as a base reference for the success of the design. The experimental results show that RosettaDesign successfully increased binding affinities by 5–7 kJ/mol above the alanine reference, but the affinities were still lower by 7–9 kJ/mol than those for the wild-type complex (Table 1).

Computational protein design methods seek to identify amino acid sequences that provide both high affinity and specificity for the designed complex. However, specificity for the top RosettaDesign pairs was not achieved. All designed proteins, except for NYP^{B}, interacted more strongly with the wild-type protein than with the designed partner (Table 1).

Computational redesign of the interface using PDB fragments

The method PDBmodDesign was specifically developed for the current study and is fundamentally different from RosettaDesign. Here, native proteins are considered to have optimal structure; thus, resolved protein structures can be an ideal resource for nature-optimized templates. In the first step, we searched for sets of five interacting residues in the PDB ("PDB modules") that have a backbone arrangement similar to that of the M2 interface module. We searched through the entire three-dimensional space of the proteins, not only through interfaces, as the interface search space was too small. Residues composing M2 are buried in the TEM1–BLIP interface, favoring such a strategy. A list of nonredundant proteins was obtained from the PISCES server (resolution of 2.5 Å or better; mutual sequence identity of less than 50%).[16] This list contained 5307 single protein chains. Whenever the protein chain was part of a larger complex, the coordinates of a whole complex were used in the search. In total, 4948 PDB entries were used.

Using only distance constraints (Fig. 1d), the search procedure identified ~10^{7} PDB modules.

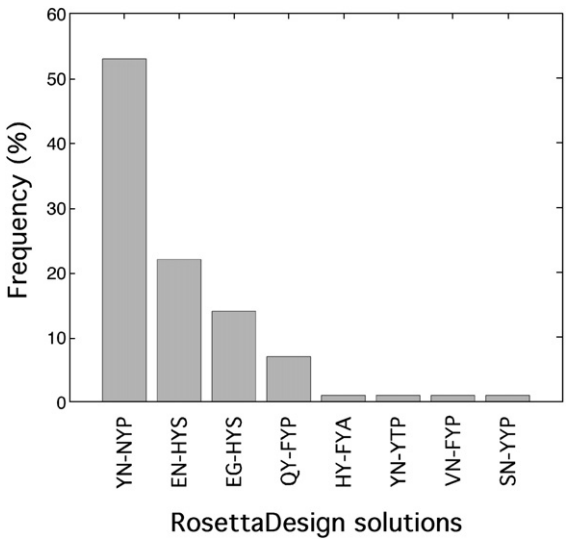

Fig. 2. RosettaDesign solutions. One hundred RosettaDesign runs (as described in Materials and Methods) converged into eight different solutions, each predicted to be energetically lower than the wild-type complex. The three most frequently occurring design solutions were experimentally evaluated.

Table 1. Loss of binding free energies determined by SPR

	TEM1–BLIP[a]	$\Delta\Delta G_{k_{off}}$[b] (kJ/mol)	$\Delta\Delta G_{K_a}$[c] (kJ/mol)
	AA–AAA	14.1	14.5[d]
A. *RosettaDesign*			
53% convergence	YN–NYP	6.9	6.3
	YN–wt	4.6	3.0
	wt–NYP	No binding	No binding
22% convergence	EN–HYS	7.6	8.9
	EN–wt	0.1	1.5
	wt–HYS	2.4	2.8
14% convergence	EG–HYS	8.1	7.6
	EG–wt	−0.4	0.4
	wt–HYS	2.4	2.8
B. *PDBmodDesign*			
Top-ranked complex	WK–QYF	0.7	−1.1
	wt–QYF	14	13[d]
	WK–wt	Weak binding	15.4[d]
Best complementarity	RY–WRY	15.4	11.5[d]
	RY–wt	15.1	12.6[d]
	wt–WRY	14.0	16.3[d]
C. *Predicted best solution without use of PDB modules*[e]			
	KK–EHF	13.0	14.0[d]
	wt–EHF	No binding	No binding
	KK–wt	No binding	No binding

[a] The first two residues are Glu104 and Tyr105 in TEM1, and the last three residues are Lys74, Phe142, and Tyr143 in BLIP. The wild-type sequence is EY–KFY.
[b] $\Delta\Delta G_{k_{off}} = -RT\ln(k_{off}^{wt}/k_{off}^{mut})$.
[c] $\Delta\Delta G_{K_a} = -RT\ln(K_a^{mut}/K_a^{wt})$.
[d] K_a values for low-affinity complexes were also determined by equilibrium analysis (see Materials and Methods; Eq. 3). The others were determined from $K_a = k_{on}/k_{off}$.
[e] The same force field was applied as for the top-ranked complex, but using any combination of residues.

However, inspection of superimposed structures demonstrated that, even in PDB modules with an RMSD of less than 1 Å, the orientation of side chains could deviate significantly from that in M2 and showed interactions considerably different from those in the target structure. Therefore, angle constraints for C^{α}–C^{β} bonds were introduced to ensure that side chains in the PDB modules point to the same directions (within 30°) as in the target module (Fig. 1d). This drastically reduced the number of acceptable modules to 361 (Supplementary Table 1). Next, the five side chains from each PDB module were remodeled within the interface context of the wild-type TEM1–BLIP complex in their respective positions, using SCCOMP.[17] Side-chain orientations of the target residues in contact with the module residues were remodeled as well.

Ranking of the 361 PDB modules was made according to their predicted complex stability upon interface remodeling. This was performed using an energy function that includes atom–atom and atom–solvent contact surfaces,[18] an electrostatic term, and side-chain volumes (see Materials and Methods). The components of the function were weighted to reproduce experimentally known $\Delta\Delta G$ values for a large set of mutations in the TEM1–BLIP interface.[11,12,19] A correlation coefficient of 0.7 was achieved between the calculated data and the experimental data (Fig. 3). Sixteen complexes are predicted to have binding energy greater than that of the wild-type complex (Fig. 4). The top-ranked complex, WK^{T}–QYF^{B}, was taken for experimental validation.

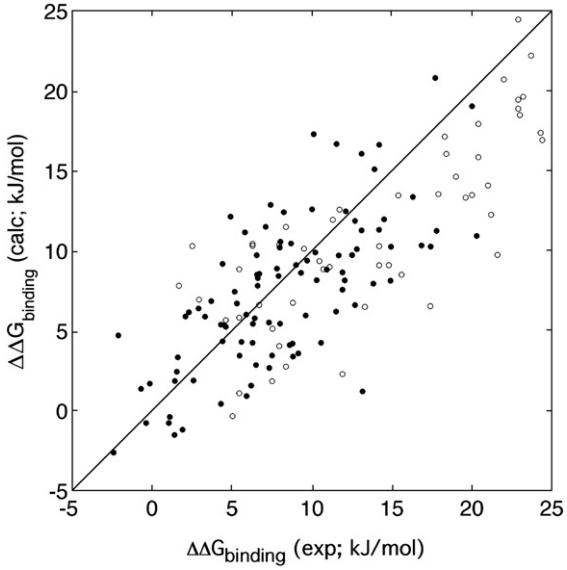

Fig. 3. Comparison of experimental and calculated $\Delta\Delta G$ values for a set of 151 mutations in the TEM1–BLIP interface. The scoring function was trained on a subset of 96 mutations (filled circles) with a correlation coefficient of 0.7. A subset of 55 mutations not used in training (empty circles) was evaluated using this scoring function. The correlation coefficient for the test set, which contained only Ala mutations, was even higher ($R = 0.78$). The overall correlation coefficient for the entire set of 151 mutations is 0.78. The continuous line represents $y = x$.

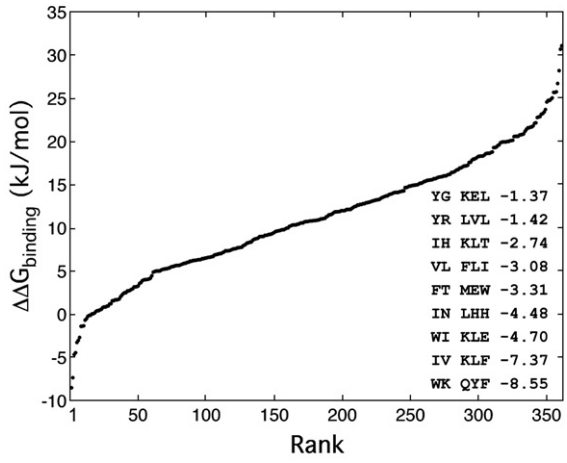

Fig. 4. Scoring the 361 PDB modules according to predicted binding free energy ($\Delta\Delta G_{binding}$) following interface remodeling. Calculations were carried out relative to the wild-type TEM1–BLIP complex ($\Delta\Delta G_{binding} = 0$). Sixteen modules have calculated $\Delta\Delta G_{binding}$ values lower than those of the wild type ($\Delta\Delta G_{binding} < 0$). The sequences of the top nine are listed. The highest-scoring module (WK^{T}–QYF^{B}) was experimentally verified (Fig. 5 and Table 1).

Experimental validation of the design

Table 1B and Fig. 5 summarize the binding free energies of the designed complexes. SPR measurements show the binding affinity of the WK^T–QYF^B complex to be equal (within the experimental error) to that of the wild type. In addition, this complex is highly specific: WK^T and QYF^B proteins interact strongly with each other, but only marginally with their wild-type counterpartners (Fig. 5c and d and Table 1B). According to SPR, the k_{off} values of the designed and wild-type complexes are 2.0×10^{-4} s^{-1} and 1.5×10^{-4} s^{-1}, respectively, with k_{on} values of 2.9×10^{5} M^{-1} s^{-1} and 1.4×10^{5} M^{-1} s^{-1} corresponding to binding affinities of 0.7 nM and 1.0 nM, respectively. In contrast, the binding affinities for wt^T–QYF^B and WK^T–wt^B as determined using the equilibrium signal (Eq. 3) were 130 nM and 330 nM. This represents a specificity switch (based on K_d) for cognate and noncognate complexes of 190-fold for wt^T–QYF^B and 480-fold for WK^T–wt^B.

While SPR is a reliable method for determining k_{off}, values of k_{on} may differ from those measured in solution.[20–23] Therefore, the association rate constant of the WK^T–QYF^B complex in solution was additionally measured using stopped-flow spectrophotometry. Using this method, the k_{on} of the designed complex was determined to be 20-fold faster than that of the wild-type complex ($9.3\times10^{6}M^{-1}$ s^{-1} *versus* 4.4×10^{5} M^{-1} s^{-1}; Supplementary Fig. 1). The k_{on} value for WK^T–wt^B was 5.5×10^{6} M^{-1} s^{-1}. Thus, the faster association rate constant of WK^T–QYF^B does not contribute to specificity, but only to the affinity of the mutant. This is among the best computational design results reported so far for transient protein–protein heterocomplexes.

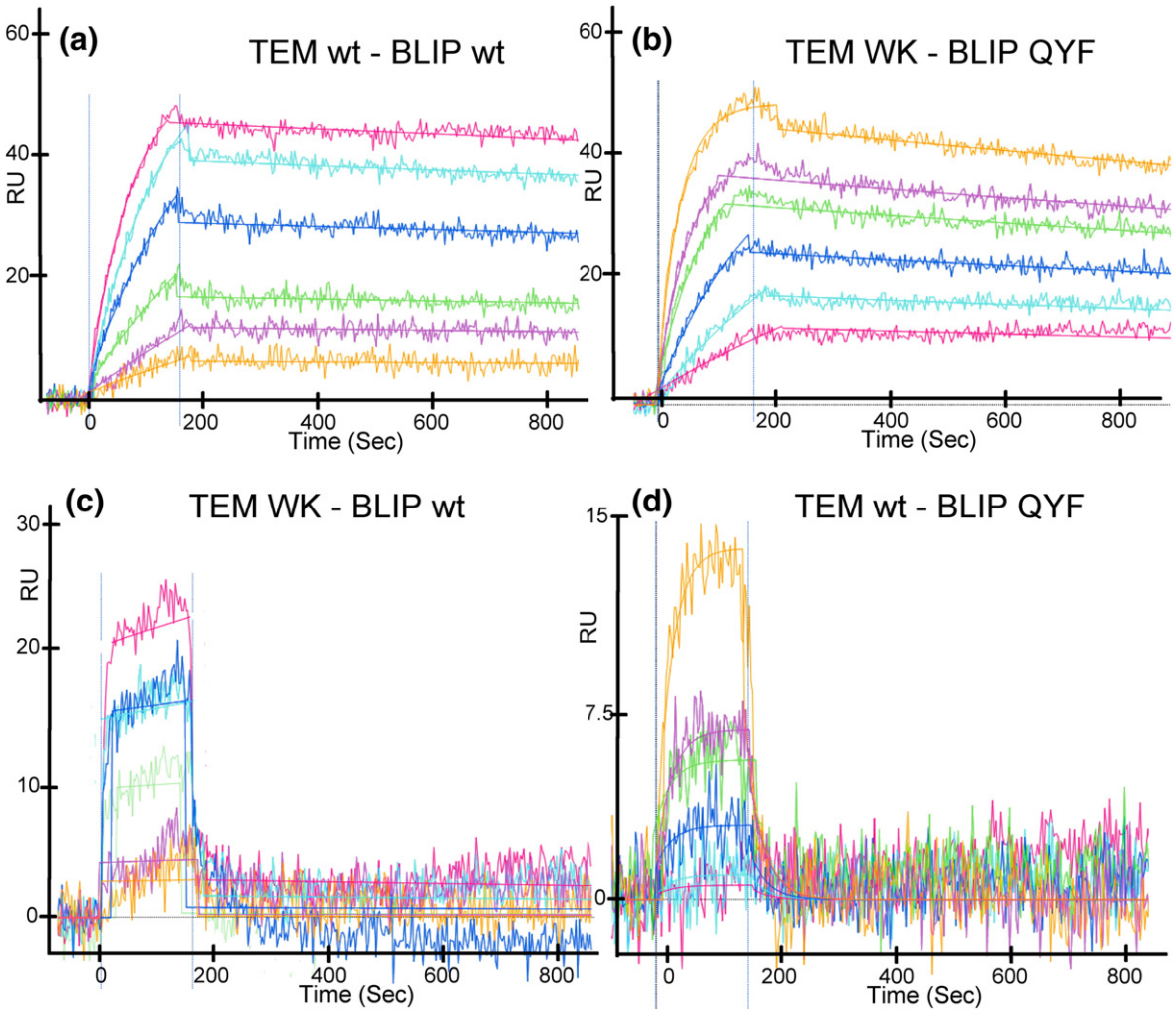

Fig. 5. Real-time binding measurements of wild-type complex (a), WK^T–QYF^B (b), WK^T–BLIP wt (c), and TEM wt–QYF^B (d). SPR measurements were carried out at six different concentrations of the BLIP protein: 5 nM, 10 nM, 20 nM, 40 nM, 60 nM, and 100 nM. The TEM protein was immobilized on the sensor chip. For wild type and WK^T–QYF^B, affinity was determined from the kinetic trace. For WK^T–BLIP wt and TEM wt–QYF^B, affinity was calculated from the equilibrium signal using Eq. 3. The plots in the figure show one binding measurement from at least three independent repeats.

Evaluating the influence of redesigning M2 on its environment

Despite major efforts, we were not able to obtain an X-ray structure of the WK^T–QYF^B complex to validate its structural integrity. While the complex crystallized readily and diffracted to high resolution, the unit cell was repeatedly too large to be solved. Therefore, as an alternative method for probing the integrity of the interface, we compared the influence of mutations from other modules on the WK^T–QYF^B complex to their influence on the wild-type complex (Fig. 6). Table 2A shows that the $\Delta\Delta G$ values for the single Ala mutations $Q99^T$, $W150^B$, $H41^B$, and $P107^T$ were similar on wild-type and WK^T–QYF^B backgrounds, while values for $S235^T$, $R243^T$, and $D49^B$ were different. These latter three residues are all located in module M1, with $D49^B$ interacting directly with the other two residues (Figs. 1b and 6).

To obtain additional information on distance constraints within the designed interface, we analyzed double-mutant cycles by comparing interaction energies between pairs of residues outside M2 that are known to be in direct contact in the resolved structure of the wild-type complex. If these residue pairs also interact in the designed complex, then it can be deduced that the distance constraints of the designed interface resemble those in wild type. The double-mutant cycle method has been previously used to validate the structural integrity of interfaces.[11,19,24] Three pairs of known wild-type interacting residues were evaluated on WK^T–QYF^B background: interactions between residues $Q99^T$–$W150^B$ (located in M3) and residues $R243^T$–$D49^B$ and $S235^T$–$D49^B$ (located in M1) (Fig. 6). Although the magnitude of interaction energies is similar to that in the wild-type background only for the $Q99^T$–$W150^B$ pair, double-mutant cycle analysis showed that significant $\Delta\Delta G_{int}$ values are obtained for all three pairs (Table 2B). Therefore, it seems that the interface is similar to that of wild type; however, the design has some influence on the energy landscape of M1.

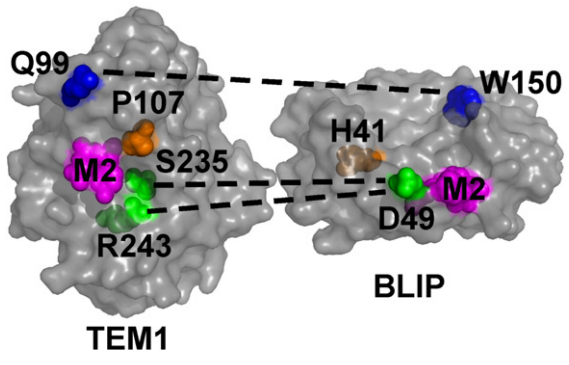

Fig. 6. Location of mutations external to M2. These mutations were used to determine whether distance constraints in wild-type and designed complexes are similar. Residue color is matched to the corresponding module color in Fig. 1a. Double-mutant cycle residues are connected by dashed lines. The five residues used in the redesign of M2 are colored. The protein surface is rendered in semitransparent gray, and experimentally probed residues are represented as spheres. The figure was generated with PyMOL.[37]

Table 2. Loss of binding free energies of alanine mutations located outside M2 on wild-type and WK^T–QYF^B backgrounds

	$\Delta\Delta G_{k_{off}}$[a] (kJ/mol)		$\Delta\Delta G_{K_a}$[b] (kJ/mol)	
	WK^T–QYF^B	wt[c]	WK^T–QYF^B	wt[c]
A. *Binding free energies*				
$Q99^T$	1.4	1.8	1.4	1.8
$P107^T$	1.3	0.7	2.4	−1.6
$S235^T$	1.2	5.5[d]	1.2	5.4[d]
$R243^T$	1.0	2.3[d]	1.0	5.8[d]
$W150^B$	13.5	15.4	13.0	17.8
$H41^B$	14.8	13.3	15.0	13.6
$D49^B$	3.0	7.1	4.7	7.0
B. *Interacting binding free energies ($\Delta\Delta G_{int}$) determined from double-mutant cycles*				
$Q99^T$–$W150^B$	−3.2	−3.9	−3.3	−3.0
$R243^T$–$D49^B$	−2.7	−5.6[d]	−4.0	−8.8[d]
$S235^T$–$D49^B$	−1.6	−6.1[d]	−1.4	−6.3[d]

The first two residues are Glu104 and Tyr105 in TEM1, and the last three residues are Lys74, Phe142, and Tyr143 in BLIP. The wild-type sequence is EY–KFY.

[a] $\Delta\Delta G_{k_{off}} = -RT\ln(k_{off}^{wt}/k_{off}^{mut})$.

[b] $\Delta\Delta G_{K_a} = -RT\ln(K_a^{mut}/K_a^{wt})$.

[c] Data for mutations on wild-type background were obtained from Reichmann *et al.*[12]

[d] Data for mutations on wild-type background were obtained from Albeck *et al.*[19] using a different SPR setup and buffer.

Only the designed residue combination retains high binding affinity

A well-known feature of protein–protein interfaces is the high degree of surface complementarity between the binding proteins.[11,12] Therefore, early on, we evaluated the combination that has the highest complementarity rank (see Materials and Methods and Supplementary Table 4) among the 361 modules, namely, RY^T–WRY^B. However, the binding affinities proved to be similar to the values obtained for the all-Ala replacement (Table 1B). Apparently, surface complementarity in a designed module is not sufficient to reproduce a stable complex—a task that requires a more accurate scoring function.

An additional 19 mutant modules, obtained by pairing components from different design experiments, were similarly tested for binding (Table 3). All of these pentamutant complexes have weak binding affinities. The reduction in the binding free energy of the strongest complex among them (YY^T–WRY^B) was 9.3 kJ/mol; however, most have affinities close to that of the all-Ala mutant, with some complexes binding below the limit of experimental detection. This result shows the difficulty in finding residue combinations involving both proteins that provide high affinity and specificity to the

Table 3. Binding free energies for nondesigned mutant modules

TEM1–BLIP[a]	$\Delta\Delta G_{k_{off}}$ [b] (kJ/mol)
A. *Binding of noncorresponding protein pairs*	
AA–FVS	10.7
AA–HYS	11.6
AA–WRY	10.7
EN–AAA	No binding
EN–FVS	No binding
EN–WRY	No binding
YN–AAA	12.6
YN–FVS	12.8
YN–HYS	10.5
YN–WRY	10.6
YY–AAA	11.2
YY–FVS	14.9
YY–HYS	10.4
YY–WRY	9.3
RY–AAA	12.9
RY–FVS	13.5
RY–HYS	15.5
WK–EHF	No binding
WK–YMH	No binding
B. *Binding with wild-type counterpartners*	
AA–wt	6.0
YY–wt	6.6
wt–AAA	No binding
wt–FVS	No binding
wt–YMH	19.5

[a] The first two residues are Glu104 and Tyr105 in TEM1, and the last three residues are Lys74, Phe142, and Tyr143 in BLIP. The wild-type sequence is EY–KFY.
[b] $\Delta\Delta G_{k_{off}} = -RT\ln(k_{off}^{wt}/k_{off}^{mut})$.

complex, as well as poor flexibility of the target module in introducing new residues.

Discussion

A central tenet in the design of complex systems is that individual components are modular. It was recently demonstrated that modularity is a fundamental design principle not only in human engineered systems but also in biological systems such as transcription activation[25] and biochemical reactions.[26] We have shown that this principle applies for protein–protein interactions as well.[11,12,27]

Here, we took advantage of the natural design principle of modularity to develop a strategy for redesigning the TEM1–BLIP interface by filling in the geometric space occupied by M2 with a different set of residues derived from a nonrelated protein found in the PDB database. The top-scoring designed complex that we obtained is highly specific. Its binding affinity is similar to that of wild type according to SPR, and even tighter than that of wild type when taking the stopped-flow data into account. The PDB module that gave the best design result for the TEM1–BLIP interface was extracted from the interior of a protein. While it has an amino acid composition overlapping the wild-type residues (WK^T–QYF^B *versus* EY^T–KFY^B), the sequence positions that they occupy are all different. A module from the protein interior could be used for interface redesign, as the chemistries of the intraprotein and interprotein interactions are similar.[28]

We failed to resolve an X-ray structure of the crystallized mutant complex as it repeatedly crystallized in intractable forms. We therefore resorted to validating its integrity by evaluating the effect of the design on the binding energy of residues located in neighboring modules. Both the single mutations and the double-mutant cycles summarized in Table 2 and Fig. 6 show that the design had no effect on residues located in M3 ($Q99^T$, $W150^B$, and their interaction) and M5 ($P107^T$ and $H41^B$). However, significant differences were detected for mutations located in M1 on a background of WK^T–QYF^B *versus* that of wild type. Still, M1 residues $R243^T$ and $D49^B$ do interact, albeit with a different energy of interaction (Table 2B), suggesting that they are in close proximity. All in all, these data show that the WK^T–QYF^B interface closely resembles that of the wild type, albeit with some changes in the interaction energies in M1.

A combination of three factors contributed to the success of our design approach: utilizing the modular architecture of the interface, employing native PDB templates, and accurate scoring function to correctly rank putative protein–protein complexes. Surprisingly, we were able to locate only a few PDB templates with similar backbone arrangements as in the wild type. From ~10^7 starting templates satisfying the distant constraints between C^α and C^β atoms in our search, none passed an angle constraint cutoff of 15°, and only 361 (Supplementary Table 1) passed a cutoff of 30°. This suggests that the precise geometric arrangement of the interacting residues in an interface module is a relatively unique feature in structure space.

The scoring function used was specifically trained on experimental data obtained from mutagenesis of interface residues in the TEM1–BLIP complex. The function allowed us to successfully rank the list of putative PDB-based complexes, while a complementarity rank gave much poorer results (Table 1B). This suggests that proper accounting of the fine details of residue–residue interactions is of major importance. The lesser success of the RosettaDesign solutions is probably due to the fact that, for the TEM1–BLIP interface, RosettaDesign failed to correctly calculate the free energy of mutations (correlation coefficient $R = 0.3$; unpublished data) between experimental and calculated $\Delta\Delta G$ values, *versus* $R = 0.7$ using our scoring function.

Ranking the list of 361 putative protein–protein complexes using our scoring function demonstrates that only a few complexes produced an energy score better than that of the wild type (Fig. 4). This suggests that only a small number of PDB modules can be successfully grafted into the TEM1–BLIP interface while retaining the same binding affinity. Accordingly, most residue combinations will destabilize the complex. Experimental data measured for 43 residue combinations (Tables 1 and 3) for M2 support this contention.

An intriguing aspect of our scoring function is its ability to correctly identify a high-affinity module on

the PDB-based list of putative protein modules, but not on a list based on artificial sequences. Using our scoring function to choose the top-ranked residue combination without the use of the PDB-based list resulted in a specific but low-binding-affinity complex (KK^T–EHF^B; $\Delta\Delta G_{k_{off}} = 13$ kJ/mol; Table 1C and Supplementary Fig. 2). It is known that energy functions may be biased toward artificial sequences that do not occur in native protein structures.[29] Therefore, employing PDB modules is advantageous as they preclude unrealistic sequences.

From the TEM1–BLIP case analyzed experimentally in this work, we cannot state that the new methodology presented here will be superior to other methods with different complexes. Rather, we consider the successful redesign of M2 in the TEM1–BLIP interface as demonstrating the feasibility of this approach at least in this particular experimental system and could be considered as a proof of concept. This approach could be generalized to redesign a whole interface by constructing it incrementally from small PDB fragments similar to the idea of using fragment libraries in Rosetta for ab initio structure prediction.[15]

A previously designed protein–protein complex achieved increased specificity but at the expense of decreased affinity.[9] Using protein engineering, we showed that it is not difficult to obtain an increased affinity for a designed partner without specificity by optimizing the electrostatic complementarity between the proteins.[30,31] Good design, however, requires both parameters simultaneously; achieving it may be more a matter of evolution than a matter of revolution.

Materials and Methods

Computational design using PDB fragments (PDBmodDesign)

Geometric search

The atomic coordinates of the five residues selected for redesign were taken from a structure of wild-type TEM1–BLIP complex (PDB ID 1JTG; resolution, 1.7 Å). These five residues (Glu104 and Tyr105 in TEM1, and Lys74, Phe142, and Tyr143 in BLIP) are referred to as the "interface module." The search procedure uses all atom–atom distances for sets of five C^α atoms and five C^β atoms in the interface module. In the first step, all possible sets of five residues in a particular PDB entry (referred as "PDB modules") are assessed to meet the distance constraints determined in the interface module. A PDB module is rejected if the difference between atom–atom distances in the interface module and the corresponding distances in the PDB module is above 2.5 Å for at least one distance (Fig. 1d). To speed up the search, distances between C^α atoms were assessed first, and only if they met these distance constrains were other distances checked. In the second step, the angle between the C^α–C^β vectors in the PDB module and the interface module was calculated after superimposition of the two modules (Fig. 1d). A PDB module was accepted only if each of the five angles was equal to or less than 30°.

Scoring function

The scoring function utilizes atom–atom contact surface areas.[18] The major underlying assumptions were that: the change in protein complex stability upon mutation is proportional to the change in the contact surface area, and proper weights can be obtained based on experimentally determined stability changes for a set of interface mutations. The scoring function was trained on mutation data previously obtained for the TEM1–BLIP protein complex[11,12,19] and on experimental data for mutants used for design in this study. Solvent-accessible area was considered as a contact with a special atom type. In addition to eight standard atom types,[18] this resulted in 36 atom–atom and 8 atom–solvent types of contact surface.

Deriving weights for all 44 contact surface types resulted in overfitting of the data. Several attempts were undertaken to utilize a computer-driven approach for selecting the best subset of contact surface types and their weights. This resulted in a scoring function with a reduced number of contact surface types that, in spite of a significant correlation factor ($R = 0.73$) for calculated data *versus* experimental data, led to designed sequences with unrealistic amino acid compositions and calculated stability change. Analysis of chosen parameters and weights in this scoring function showed that the contact surface between atoms of the neutral/donor class was close to zero in the training set, resulting in spurious random correlations.

Instead of the above, a scheme that includes all atom–atom and atom–solvent contact surfaces, grouped according to their physical–chemical compatibility, was developed.[32] Using contact surface types highlighted one general problem: some contact surface types are completely absent in the training set, and the proper weights just cannot be derived. Interactions between negatively (or positively) charged groups are very rare in proteins and protein complexes, as they are destabilizing in nature. On the other hand, in the design procedure, a proper weight must be used to punish such interactions. This situation was resolved by summing up rare contacts, with frequent ones having an opposite sign such that the same weight is given to rare contacts but with opposite sign. The scoring function includes 14 groups of atom–atom contacts (Fig. 7).

Note that charge–charge interactions are about twice as strong as polar–charge interactions and about four times stronger than polar–polar ones.[33] Therefore, polar–charge contacts were counted twice, and charge–charge interactions were counted four times to give a higher weight to these types of interactions. The donor–aromatic contact surface type (positively charged atoms in Lys and Arg in contact with an aromatic ring) was counted twice as well, as it represents π–cation interactions having increased strength. Giving higher weights to these types of interactions proved to be in the right direction, as it resulted in an increase in the correlation coefficient between the calculated data and the experimental data. Equal weights were assumed for any atom–solvent contacts and any atom–hydrophilic contacts. Thus, they were summed into one term for each atom type (acceptor/solvent with acceptor/hydrophilic, donor/solvent with donor/hydrophilic, and so on).

Two additional terms were introduced to the scoring function, as their effect was not captured by the surface complementarity approach: an explicit electrostatic term[31] and a side-chain volume term. The side-chain volume term accounts for the packing of residues and was calculated as the sum of amino acid volumes.[34] The entropy term, surprisingly, had negligible contribution and was not included in the scoring function. Similar results have

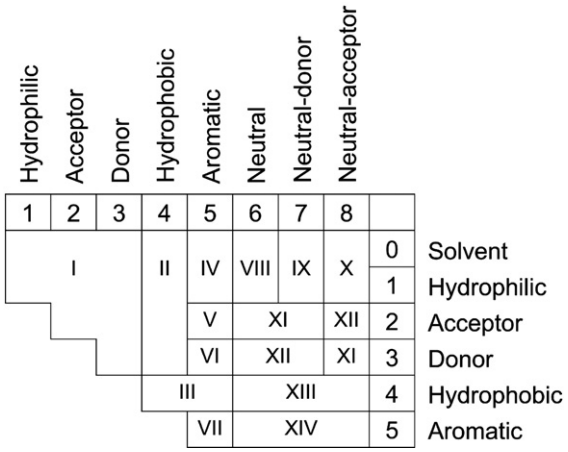

Fig. 7. Grouping of contact surface types (Roman numerals) in the scoring function. Solvent-accessible surface was considered as contact with a special atom type (type 0), in addition to eight standard atoms types.[32] Thirty-six atom–atom and eight atom–solvent types of contact surface were sorted into 14 groups according to physical–chemical compatibility: (I) hydrophilic/hydrophilic, hydrophilic/acceptor, hydrophilic/donor, acceptor/donor, acceptor/acceptor with opposite sign, donor/donor with opposite sign; (II) hydrophobic/hydrophilic, hydrophobic/acceptor, hydrophobic/donor; (III) hydrophobic/hydrophobic, hydrophobic/aromatic; (IV) aromatic/hydrophilic; (V) aromatic/acceptor; (VI) aromatic/donor; (VII) aromatic/aromatic; (VII) hydrophilic/neutral; (IX) hydrophilic/neutral donor; (X) hydrophilic/neutral acceptor; (XI) acceptor/neutral, acceptor/neutral donor, donor/neutral acceptor; (XII) donor/neutral, donor/neutral acceptor, acceptor/neutral acceptor; (XIII) hydrophobic/neutral, hydrophobic/neutral donor, hydrophobic/neutral acceptor; (XIV) aromatic/neutral, aromatic/neutral donor, aromatic/neutral acceptor. Note that contacts among neutral atom types are infrequent and were not included in the scoring function.

recently been reported.[35] The resulting scoring function, trained on mutational data for the TEM1–BLIP protein complex, had a correlation coefficient $R=0.70$. The performance of the scoring function was tested on a set of 55 mutations of the TEM1–BLIP complex that was not used in training. The correlation coefficient of this set, which contained only Ala mutations, was even higher ($R=0.78$).

The binding energy ($\Delta\Delta G_{\text{binding}}$) was calculated by evaluating wild-type (wt) and mutant (mut) proteins in the complex and in the unbound form:

$$\begin{aligned}\Delta\Delta G_{\text{binding}} &= \Delta G^{\text{mut}}_{\text{binding}} - \Delta G^{\text{wt}}_{\text{binding}} \\ \Delta G_{\text{binding}} &= \Delta G_{\text{complex}} - \left(\Delta G_{\text{protein A}} + \Delta G_{\text{protein B}}\right)\end{aligned} \quad (1)$$

Side chains were modeled in their correct environment (in the complex and in unbound proteins) using the SCCOMP program.[17] Residues in contact with mutated positions were remodeled as well.

Complementarity rank

Several parameters were defined for every PDB module based on a surface complementarity approach.[18] S_{clu} is the surface area sum of all atom–atom contacts between residues forming the module, with appropriate sign; S_{env} is the surface area sum of all atom–atom contacts between residues from the module and from the environment; and S_{int} is the surface area sum of all atom–atom contacts between residues in the module, but from different chains. The last parameter was introduced to ensure that residues from different protein chains form substantial contacts. Every PDB module was assigned a rank according to its S_{clu}, S_{env}, and S_{int} values, and total rank (complementarity rank) was defined as the sum of the three ranks.

Computational design by RosettaDesign

The variant library was designed using the RosettaDesign program,[13] with the crystal structure of wild-type TEM1–BLIP complex (PBD ID 1JTG; chains A and B) as starting template. Calculations were carried out to evaluate combinatorial substitutions of five residues in the interface module M2. In each case, amino acids contacting the substituted residues were repacked (allowing all rotamers of the native amino acid type). The program was run 100 times, and final residue sets were selected as the most repetitive results.

Site-directed mutagenesis

Mutagenesis was performed using Kunkel mutagenesis based on single-stranded DNA, as described before.[11] Insertion of mutations was verified by DNA sequencing.

Protein expression and purification

Expression and purification of TEM1 and BLIP were undertaken as described.[22] The quality of protein (degree of purity and activity), as well as its relative concentration, was determined alone and in complex with wild-type protein using analytical gel-filtration chromatography.

Kinetic measurements

Kinetic constants were evaluated by SPR detection using the ProteOn™ XPR36 Protein Interaction Array System (Bio-Rad) in phosphate-buffered saline (pH 7.4) with 0.005% surfactant P20 at 25 °C. For all measurements, TEM1 was immobilized by amine coupling to the sensor chip, and BLIP was the analyte applied at six different protein concentrations simultaneously. Data were analyzed with BIAeval 4.1 software using both Langmuir models for fitting kinetic data (global and local fitting) and, from the equilibrium response at each concentration, fitted to the mass–action equation. The change in free energy ($\Delta\Delta G_{K_a}$) upon mutation was calculated from:

$$\Delta\Delta G_{K_a} = -RT\ln\frac{K_a^{\text{mut}}}{K_a^{\text{wt}}} \quad (2)$$

with K_a values being determined in two ways: by the ratio of the kinetic constants ($K_a = k_{on}/k_{off}$; for interactions of $k_{on} < 5\times10^6$ M^{-1} s^{-1} and $k_{off} < 0.2$ s^{-1}), and by following the change in the refractive index (RU) at the equilibrium-binding signal and then by fitting the data to the mass action expression ($K_{a(ma)}$):

$$\text{RU} = \left[CK_{a(ma)}R_{\max}\right]/\left[CK_{a(ma)}+1\right] \quad (3)$$

where C represents the protein concentration. Values of $\Delta\Delta G_{K_a}$ (determined from k_{on}/k_{off}) and $\Delta\Delta G_{K_a(ma)}$

(determined by mass action) are highly correlated ($R=0.99$). Error analysis shows that significant values of $\Delta\Delta G$ (2SE) calculated from k_{off} were >0.7 kJ/mol, and those from K_a were >1.4 kJ/mol.[11,36]

Double-mutant cycle analysis

The interaction binding energy $\Delta\Delta G_{int}$ for a pair of residues (residues 1 and 2) was calculated from:

$$\Delta\Delta G_{int} = \Delta\Delta G^{mut1mut2} - \Delta\Delta G^{mut1} - \Delta\Delta G^{mut2} \quad (4)$$

This analysis reveals whether the contributions from a pair of residues are additive, or whether the effects of mutations are coupled. If there is no interaction between the two mutated residues, the effects of the two substitutions should be additive in respect to the double mutation ($\Delta\Delta G_{int}=0$). If they form an attractive interaction, the interaction binding energy is negative ($\Delta\Delta G_{int}<0$), and a repulsive interaction results in a positive interaction energy ($\Delta\Delta G_{int}>0$). The experimental error for $\Delta\Delta G_{int}$ (2SE) calculated from k_{off} is 1.2 kJ/mol, and that from K_a is 2.4 kJ/mol.

Acknowledgements

This study was supported by Israel Ministry of Science and Technology grant 263 to G.S., M.E., and V.S., and by MINERVA grant 8525 to G.S.

Supplementary Data

Supplementary data associated with this article can be found, in the online version, at doi:10.1016/j.jmb.2008.08.078

References

1. Cusick, M. E., Klitgord, N., Vidal, M. & Hill, D. E. (2005). Interactome: gateway into systems biology. *Hum. Mol. Genet.* **14**(Spec. Publ. No. 2), R171–R181.
2. Crameri, A., Cwirla, S. & Stemmer, W. P. (1996). Construction and evolution of antibody-phage libraries by DNA shuffling. *Nat. Med.* **2**, 100–102.
3. Hanes, J. & Plückthun, A. (1997). *In vitro* selection and evolution of functional proteins by using ribosome display. *Proc. Natl Acad. Sci. USA*, **94**, 4937–4942.
4. Binz, H. K. & Plückthun, A. (2005). Engineered proteins as specific binding reagents. *Curr. Opin. Biotechnol.* **16**, 459–469.
5. Kortemme, T. & Baker, D. (2004). Computational design of protein–protein interactions. *Curr. Opin. Chem. Biol.* **8**, 91–97.
6. Clark, L. A., Boriack-Sjodin, P. A., Eldredge, J., Fitch, C., Friedman, B., Hanf, K. J. M. *et al.* (2006). Affinity enhancement of an *in vivo* matured therapeutic antibody using structure-based computational design. *Protein Sci. Publ. Protein Soc.* **15**, 949–960.
7. Sammond, D. W., Eletr, Z. M., Purbeck, C., Kimple, R. J., Siderovski, D. P. & Kuhlman, B. (2007). Structure-based protocol for identifying mutations that enhance protein–protein binding affinities. *J. Mol. Biol.* **371**, 1392–1404.
8. Song, G., Lazar, G. A., Kortemme, T., Shimaoka, M., Desjarlais, J. R., Baker, D. & Springer, T. A. (2006). Rational design of intercellular adhesion molecule-1 (ICAM-1) variants for antagonizing integrin lymphocyte function-associated antigen-1-dependent adhesion. *J. Biol. Chem.* **281**, 5042–5049.
9. Kortemme, T., Joachimiak, L. A., Bullock, A. N., Schuler, A. D., Stoddard, B. L. & Baker, D. (2004). Computational redesign of protein–protein interaction specificity. *Nat. Struct. Mol. Biol.* **11**, 371–379.
10. Joachimiak, L. A., Kortemme, T., Stoddard, B. L. & Baker, D. (2006). Computational design of a new hydrogen bond network and at least a 300-fold specificity switch at a protein–protein interface. *J. Mol. Biol.* **361**, 195–208.
11. Reichmann, D., Cohen, M., Abramovich, R., Dym, O., Lim, D., Strynadka, N. C. & Schreiber, G. (2007). Binding hot spots in the TEM1–BLIP interface in light of its modular architecture. *J. Mol. Biol.* **365**, 663–679.
12. Reichmann, D., Rahat, O., Albeck, S., Meged, R., Dym, O. & Schreiber, G. (2005). The modular architecture of protein–protein binding interfaces. *Proc. Natl Acad. Sci. USA*, **102**, 57–62.
13. Dantas, G., Kuhlman, B., Callender, D., Wong, M. & Baker, D. (2003). A large scale test of computational protein design: folding and stability of nine completely redesigned globular proteins. *J. Mol. Biol.* **332**, 449–460.
14. Moult, J. (2005). A decade of CASP: progress, bottlenecks and prognosis in protein structure prediction. *Curr. Opin. Struct. Biol.* **15**, 285–289.
15. Rohl, C. A., Strauss, C. E., Misura, K. M. & Baker, D. (2004). Protein structure prediction using Rosetta. *Methods Enzymol.* **383**, 66–93.
16. Wang, G. & Dunbrack, R. L. J. (2003). PISCES: a protein sequence culling server. *Bioinformatics*, **19**, 1589–1591.
17. Eyal, E., Najmanovich, R., McConkey, B. J., Edelman, M. & Sobolev, V. (2004). Importance of solvent accessibility and contact surfaces in modeling side-chain conformations in proteins. *J. Comput. Chem.* **25**, 712–724.
18. Sobolev, V., Wade, R. C., Vriend, G. & Edelman, M. (1996). Molecular docking using surface complementarity. *Proteins*, **25**, 120–129.
19. Albeck, S., Unger, R. & Schreiber, G. (2000). Evaluation of direct and cooperative contributions towards the strength of buried hydrogen bonds and salt bridges. *J. Mol. Biol.* **298**, 503–520.
20. Deinum, J., Gustavsson, L., Gyzander, E., Kullman-Magnusson, M., Edström, A. & Karlsson, R. (2002). A thermodynamic characterization of the binding of thrombin inhibitors to human thrombin, combining biosensor technology, stopped-flow spectrophotometry, and microcalorimetry. *Anal. Biochem.* **300**, 152–162.
21. Piehler, J. & Schreiber, G. (1999). Biophysical analysis of the interaction of human IFNAR2 expressed in *E. coli* with IFNalpha2. *J. Mol. Biol.* **289**, 57–67.
22. Albeck, S. & Schreiber, G. (1999). Biophysical characterization of the interaction of the beta-lactamase TEM-1 with its protein inhibitor BLIP. *Biochemistry*, **38**, 11–21.
23. Slepenkov, S. V., Darzynkiewicz, E. & Rhoads, R. E. (2006). Stopped-flow kinetic analysis of eIF4E and phosphorylated eIF4E binding to cap analogs and capped oligoribonucleotides: evidence for a one-step binding mechanism. *J. Biol. Chem.* **281**, 14927–14938.

24. Horovitz, A. & Fersht, A. R. (1990). Strategy for analysing the co-operativity of intramolecular interactions in peptides and proteins. *J. Mol. Biol.* **214**, 613–617.
25. Crosson, S., McGrath, P. T., Stephens, C., McAdams, H. H. & Shapiro, L. (2005). Conserved modular design of an oxygen sensory/signaling network with species-specific output. *Proc. Natl Acad. Sci. USA*, **102**, 8018–8023.
26. Papin, J. A., Reed, J. L. & Palsson, B. O. (2004). Hierarchical thinking in network biology: the unbiased modularization of biochemical networks. *Trends Biochem. Sci.* **29**, 641–647.
27. Rahat, O., Yitzhaky, A. & Schreiber, G. (2008). Cluster conservation as a novel tool for studying protein–protein interactions evolution. *Proteins*, **71**, 621–630.
28. Cohen, M., Reichmann, D., Neuvirth, H. & Schreiber, G. (2008). Similar chemistry, but different bond preferences in inter- *versus* intra-protein interactions. *Proteins*, **72**, 741–753.
29. Pokala, N. & Handel, T. M. (2001). Review: protein design—where we were, where we are, where we're going. *J. Struct. Biol.* **134**, 269–281.
30. Kiel, C., Selzer, T., Shaul, Y., Schreiber, G. & Herrmann, C. (2004). Electrostatically optimized Ras-binding Ral guanine dissociation stimulator mutants increase the rate of association by stabilizing the encounter complex. *Proc. Natl Acad. Sci. USA*, **101**, 9223–9228.
31. Selzer, T., Albeck, S. & Schreiber, G. (2000). Rational design of faster associating and tighter binding protein complexes. *Nat. Struct. Biol.* **7**, 537–541.
32. Sobolev, V., Sorokine, A., Prilusky, J., Abola, E. E. & Edelman, M. (1999). Automated analysis of interatomic contacts in proteins. *Bioinformatics*, **15**, 327–332.
33. Wesson, L. & Eisenberg, D. (1992). Atomic solvation parameters applied to molecular dynamics of proteins in solution. *Protein Sci. Publ. Protein Soc.* **1**, 227–235.
34. Zamyatnin, A. A. (1972). Protein volume in solution. *Prog. Biophys. Mol. Biol.* **24**, 107–123.
35. Hu, X. & Kuhlman, B. (2006). Protein design simulations suggest that side-chain conformational entropy is not a strong determinant of amino acid environmental preferences. *Proteins*, **62**, 739–748.
36. Reichmann, D., Phillip, Y., Carmi, A. & Schreiber, G. (2008). On the contribution of water-mediated interactions to protein-complex stability. *Biochemistry*, **47**, 1051–1060.
37. DeLano, W. L. (2007). The PyMOL Molecular Graphics System DeLano Scientific LLC, Palo Alto, CA, USA; http://www.pymol.org.